Received: 31 December 2024 | Revised: 27 November 2025 | Accepted: 4 December 2025

DOI: 10.1002/esp.70226

RESEARCH ARTICLE

ESPL WILEY

# Integrated early warning method for landslide acceleration and expansion based on GB-InSAR monitoring

Ting Xiao [1,2] | Weiming Tian [3] | Samuele Segoni [4] | Emanuele Intrieri [4] | Yunkai Deng [3] | Yunping Liao [1,2,5]

[1]Key Laboratory of Metallogenic Prediction of Nonferrous Metals and Geological Environment Monitoring (Central South University), Ministry of Education, Changsha, China

[2]School of Geosciences and Info-Physics, Central South University, Changsha, China

[3]School of Information and Electronics, Beijing Institute of Technology, Beijing, China

[4]Department of Earth Sciences, University of Florence, Florence, Italy

[5]Technology Innovation Center of Geohazards Automatic Monitoring, Ministry of Natural Resources (Chongqing Institute of Geology and Mineral Resources), Chongqing, China

**Correspondence**
Yunkai Deng, School of Information and Electronics, Beijing Institute of Technology, Beijing 100081, China.
Email: yunkai_bit@bit.edu.cn

**Funding information**
National Natural Science Foundation of China, Grant/Award Number: 42307275; Natural Science Foundation of Hunan Province, China, Grant/Award Number: 2024JJ6498; Technology Innovation Center of Geohazards Automatic Monitoring, Grant/Award Number: TICG-K2024008

## Abstract

Real-time monitoring and early warning systems for landslides are crucial for minimizing casualties and property losses. The tangential angle method, which assesses the deformation rate of the displacement–time curve at specific instances, has been successfully applied in some cases. However, this method often results in omissions, false alarms and frequent alerts due to its reliance on fixed time windows and single-point displacement measurements. Ground-Based Interferometric Synthetic Aperture Radar (GB-InSAR) is an advanced deformation monitoring technology offering high frequency and accuracy. Nonetheless, it currently lacks a quantitative early warning method that fully leverages surface scene information. To address these challenges, this paper proposes a hybrid intelligent early warning approach based on surface deformation monitoring, comprising a point-based early warning (PEW) method and an area-based early warning (AEW) method. The PEW method enhances the traditional tangential angle approach by adopting a self-adaptive time window, thereby reducing warning errors associated with fixed time intervals. The AEW method facilitates early warnings by detecting landslide expansion behaviours, effectively utilizing the extensive data from surface scene monitoring. The proposed early warning system was validated through a detailed case study of the Jianshan landslide monitored by GB-InSAR. The results demonstrate that both PEW and AEW methods perform effectively within their respective scopes, although each possesses certain information blind spots. The integrated method capitalizes on the strengths of both approaches while mitigating their individual limitations, thereby achieving more accurate and reliable early warnings.

KEYWORDS
GB-InSAR, hybrid intelligent approach, landslide early warning, surface deformation monitoring, tangential angle method

## 1 | INTRODUCTION

Landslides are a type of 'mass wasting', which refers to any downslope movement of soil and rock driven by gravity and influenced by external factors such as rainfall, earthquakes and human engineering activities (Cruden & Varnes, 1996). Prior to destabilization, landslides undergo an evolutionary process during which various fields, including deformation, stress, temperature and hydrological conditions, change over time (Crosta et al., 2017; Intrieri, Bardi, et al., 2017). Based on extensive experimental statistical analysis, Saito proposed a three-stage deformation theory for the creep and progressive failure of landslides, indicating that landslides exhibit three distinct deformation phases: (1) initial deformation, (2) constant deformation and (3) accelerated deformation (Saito, 1969; Saito & Uesawa, 1966). This theory has been validated and refined by numerous researchers, with the accelerated deformation phase further subdivided into initial acceleration, mid-term acceleration, and high-speed acceleration stages (Cignetti et al., 2023; Pecoraro et al., 2018; Xu et al., 2020; Zhang, Tang, Li, et al., 2024). Consequently, throughout the entire process of landslide development and failure, surface deformation exhibits consistent and predictable patterns. These characteristic features can be utilized for the early warning and forecasting of landslides.

Early warning criteria for landslides based on surface deformation monitoring primarily include cumulative deformation, deformation rate, deformation acceleration and the tangent angle of the displacement–time curve, among others (Dixon et al., 2018; Eberhardt et al., 2012; Zhang, Tang, Tan, et al., 2024). Jibson et al. (2000) utilized landslide inventories and displacement data from the 1994 North Ridge earthquake in California to develop a probability curve that correlates displacement with the likelihood of failure. Yin et al. (2010) introduced a demonstration station system implemented in Wushan New City within the Three Gorges Reservoir area for real-time monitoring and early warning of geological disasters, where deformation rate is identified as one of the most critical indicators for early warning. Macciotta et al. (2015) described a hazard early warning system that focuses on monitoring the annual displacement cycles and potential acceleration of landslides. Landslides exhibiting different geotechnical characteristics and deformation patterns show considerable variability in their cumulative deformation, rate and acceleration thresholds during their evolutionary stages, making it challenging to establish threshold values that are universally applicable to most landslides (Crosta & Agliardi, 2002; Wu et al., 2021; Wang, Qiu, et al., 2022). Consequently, when applying rate or acceleration thresholds for early warning, professionals often need to rely on their expertise and specific case conditions for secondary assessments, resulting in these methods having limited automation and intelligence.

The tangent angle is a quantitative criterion proposed by Xu et al. (2011), defined as the ratio of the short-term deformation rate to the average rate during the constant deformation phase. Being dimensionless and exhibiting consistent threshold values across different cases, the tangent angle has increasingly been applied in landslide early warning systems. Fan et al. (2019) utilized predefined tangent angle thresholds for rockslides in their early warning system, successfully forecasting a catastrophic rockslide 53 minutes in advance. Ju et al. (2020) applied the tangent angle to the early warning of the Baige debris flow landslide, Xinyi landslide and Heifangtai landslide group, demonstrating the method's high feasibility.

The tangent angle has been successfully applied in many landslide early warning cases (Bai et al., 2022; Fan et al., 2014; Gu et al., 2023; Tan et al., 2023; Wang, Zhong, et al., 2022). However, in practical applications, the use of this method often results in missed detections or false alarms. This issue arises primarily from two factors. Firstly, the tangent angle values are highly sensitive to the monitoring frequency (i.e. the time window used in the calculations). When there is a mismatch between the monitoring frequency and the deformation frequency, particularly during the initial stages of minor deformation, this problem becomes more pronounced. Secondly, the tangent angle method is a point-based early warning (PEW) approach that effectively characterizes the deformation state in the vicinity of the monitoring equipment but fails to capture the overall deformation characteristics of the entire landslide. Additionally, monitoring devices, such as Global Navigation Satellite Systems (GNSS), are typically installed on slopes before landslide events and are not necessarily positioned in areas experiencing intense deformation. This placement strategy can easily lead to missed detections or false alarms.

In recent years, slope deformation monitoring technologies have advanced rapidly, encompassing satellite remote sensing, laser scanning, unmanned aerial vehicle remote sensing, fibre Bragg grating sensors and ground-based interferometric synthetic aperture radar (GB-InSAR), etc. (Bardi et al., 2016; Carlà et al., 2019; Han et al., 2023; Meng et al., 2020; Woods et al., 2021). Notably, GB-InSAR stands out as a cutting-edge deformation monitoring tool, offering high frequency, high precision and wide-area measurement capabilities (Dumperth et al., 2016; Intrieri, Raspini, et al., 2017; Nava et al., 2024; Tian et al., 2019; Xiao et al., 2021). Its practical value has been validated in landslide cases (Crosta et al., 2017; Dick et al., 2015; Strząbała et al., 2024). While monitoring techniques have transitioned from point-based to area-wide surveillance, corresponding early warning methods have not kept pace. Currently, there is a lack of quantitative landslide early warning approaches that fully leverage area-wide monitoring data. Therefore, developing an early warning method based on surface area monitoring information is of paramount importance.

In conclusion, although point-based tangential angle early warning methods are widely utilized, they present notable limitations. Simultaneously, there is a pressing need to develop area-based monitoring early warning approaches. This study leverages time-series deformation data from GB-InSAR monitoring of the Jianshan landslide to identify the shortcomings of the tangential angle method. In response, we have enhanced the approach by proposing an improved PEW method. Furthermore, based on the deformation patterns observed during the landslide failure process, we introduce an area-based early warning (AEW) method. This innovative approach represents a significant advance, fully utilizing surface area monitoring data. Finally, by integrating both PEW and AEW methods, we establish a comprehensive early warning framework.

## 2 | METHODOLOGY

### 2.1 | GB-InSAR system

GB-InSAR is an advanced remote sensing technique that enables high-resolution measurements of surface displacement. By analyzing the phase differences between transmitted and received signals, GB-InSAR generates detailed deformation maps of the monitored area. In these maps, each pixel corresponds to a specific displacement value, which can be used to assess surface deformation. The deformation maps produced by the GB-InSAR system offer valuable insights into processes such as subsidence or uplift over time, making them essential for monitoring geohazards and environmental changes. Its high precision and temporal resolution are crucial for understanding the dynamics of these hazards.

### 2.2 | Integrated early warning method

The occurrence and development of landslides typically unfold over time. Initially, deformation occurs locally, with the deformation zone gradually expanding until the slip surface is formed, leading to complete failure. Concurrently, the deformation and failure of the landslide often exhibit a three-phase characteristic: 'initiation–steady

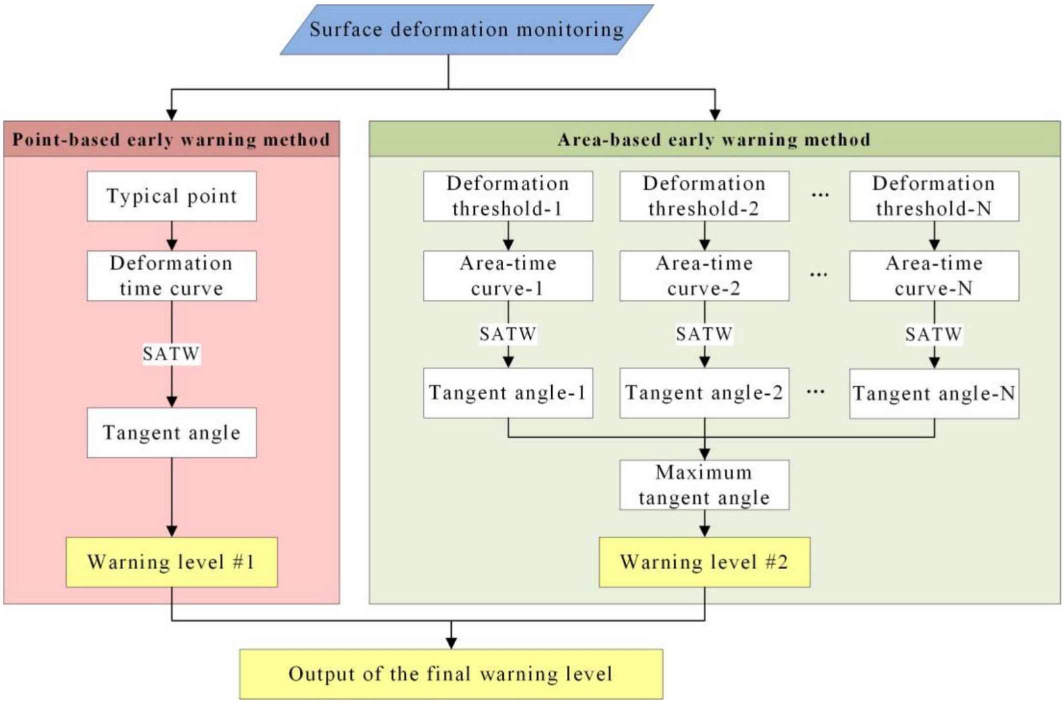


**FIGURE 1** The proposed integrated early warning method.

motion–acceleration'. Therefore, identifying the patterns of landslide deformation velocity and changes in the deformation area is crucial for early warning and forecasting. Based on this, this paper proposes an integrated early warning method, which consists of two components, namely, PEW method and AEW method, as shown in Figure 1. To detect early signs of displacement, the PEW method employs a self-adaptive time window (SATW) technique to calculate the tangential angle of the displacement–time curve for selected points within the monitored area. Warnings are issued based on the tangential angle values and predefined warning levels. Meanwhile, the AEW method uses multiple deformation thresholds to track the expansion of the deformation zone. Any area exceeding the deformation threshold is continuously monitored to generate an area–time curve. SATW is then applied again to calculate the tangential angle of the area–time curve, and another warning is issued based on the relationship between the tangential angle and the warning levels. At each time point, the more severe warning between those issued by the PEW and AEW methods will be selected as the final warning result. The following two sections will provide a detailed explanation of the principles and formulas underlying the PEW and AEW methods.

### 2.2.1 | PEW method

Based on the three-stage deformation characteristics of landslides, researchers have proposed various early warning methods. Among these, the tangent angle early warning method proposed by Xu et al. (2011) (hereafter referred to as the traditional tangent angle method) has demonstrated good application results (Liu, Yang, et al., 2024; Wang, Zhong, et al., 2022). However, our research has identified two critical issues with this method. First, the traditional tangent angle formula calculates the tangent angle using the average velocity of the second stage (i.e., the constant deformation stage) as the denominator. In real-time monitoring, it is difficult to accurately and quickly determine which stage the deformation is in. Second, the traditional method uses monitoring frequency as the time window, but the monitoring frequency varies across different devices and scenarios. This variation in frequency directly affects the size of the time window and, consequently, the calculation results. The PEW method proposed in this paper is an optimized version based on the traditional tangent angle method, which addresses these two critical issues. Next, a brief introduction to the traditional tangent angle method is provided, followed by a detailed explanation of the proposed PEW method.

1. The traditional tangent angle method

$$T_i = \frac{S_i}{v} \tag{1}$$

In essence, the tangent angle is the arctangent of the ratio of short-term velocity to average velocity. The specific formula is as follows (Xu et al., 2011, 2020):where $S_i$ represents the cumulative displacement at time $t_i$ and $v$ is the average velocity during the constant deformation stage.

Based on the $T$–$t$ curve, the tangential angle $\alpha_i$ can be calculated as

$$\alpha_i = arctan\frac{\Delta T}{\Delta t} = arctan\frac{T_i - T_{i-1}}{t_i - t_{i-1}} = arctan\frac{S_i - S_{i-1}}{(t_i - t_{i-1})\cdot v} \tag{2}$$

where $\alpha_i$ is the tangential angle on the $T$–$t$ curve, $\Delta t$ is the time window and $t_i$ is the $i$th monitoring time.

These two formulas enable the calculation of the tangential angle $\alpha_i$ at each moment during real-time landslide monitoring. Using the multiple warning criteria based on the tangential angle, as presented in Table 1, the landslide early warning level can be determined.

**TABLE 1** Multiple warning criteria based on the tangential angle.

| Tangential angle | $\alpha < 45^\circ$ | $\alpha = 45^\circ$ | $45^\circ \le \alpha < 80^\circ$ | $80^\circ \le \alpha < 85^\circ$ | $\alpha > 85^\circ$ |
|---|---|---|---|---|---|
| Warning level | Safety | Attention | Caution | Vigilance | Alarm |

2. The PEW method

The PEW method replaces the average velocity $v$ of the constant deformation stage in Equation (1) with the average velocity of the entire process. Therefore, the average velocity $B_i$ at the moment $t_i$ is calculated as follows:

$$B_i = \frac{S_i - S_1}{t_i - t_1} \tag{3}$$

where $S_i$ refers to the cumulative deformation at the time $t_i$ and $S_1$ is the initial deformation at the onset of monitoring at time $t_1$.

Next, the cumulative deformation $S_i$ is divided by the average rate $B_i$ to obtain $T_i$, which has the same dimension as time $t$, as given by the following expression:

$$T_i = \frac{S_i}{B_i} \tag{4}$$

Finally, the tangential angle $\alpha_i$ on the $T$–$t$ curve is calculated as

$$\alpha_i = arctan\frac{\Delta T}{\Delta t} = arctan\frac{T_i - T_{i-n}}{t_i - t_{i-n}} = arctan\frac{S_i - S_{i-n}}{B_i \cdot (t_i - t_{i-n})} \tag{5}$$

where $\Delta t$ is the optimal time window determined by SATW method, $S_i$ is the cumulative deformation at time $t_i$, $S_{i-n}$ is the cumulative deformation at time $t_{i-n}$ and $t_{i-n}$ is determined by the size of SATW.

3. The SATW method

The STAW method selects the optimal time window by setting multiple consecutive values as a pool for the time window $\Delta t$. The time window $\Delta t$ is defined as a sequence of $m$ consecutive values, expressed as

$$\Delta t_j = j,\ j = 1,2,3,\ldots,m \tag{6}$$

where $\Delta t$ is in hours and $m$ is typically set to 10 in most cases. For each time window, the tangential angle curve is calculated. The optimal warning time window is then identified by analyzing the overlap rate of the tangential angle curves. The identified optimal time window is incorporated into Equation (5) to calculate the tangential angle $\alpha_i$.

The tangential angle $\alpha_{i,j}$ corresponding to the time window $\Delta t_j$ is calculated by

$$\alpha_{i,j} = arctan\frac{\Delta T_j}{\Delta t_j} \tag{7}$$

where $\Delta T_j$ represents the change in $T$ within the time window $\Delta t_j$ on the $T$–$t$ curve.

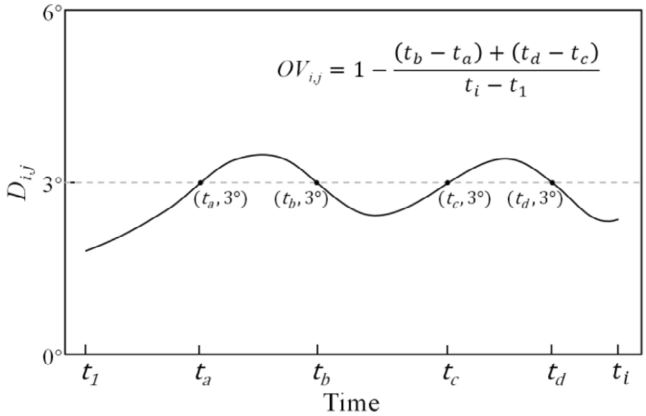


**FIGURE 2** The relationship between $OV_{i,j}$ and $D_{i,j}$.

Next, the tangential angle difference $D_{i,j}$ for two adjacent time windows at each time step is calculated as

$$D_{i,j} = |\alpha_{i,j} - \alpha_{i,j+1}| \tag{8}$$

where $\alpha_{i,j}$ is the tangential angle calculated using the time window $\Delta t_j$ at time $t_i$ and $\alpha_{i,j+1}$ is the tangential angle calculated using the time window $\Delta t_{j+1}$ at time $t_i$.

If $D_{i,j} \le 3^\circ$, the tangential angle curves $\alpha_{i,j} - t$ and $\alpha_{i,j+1} - t$ are considered to overlap. The overlap ratio $OV_{i,j}$ is defined as the ratio of the overlapping time to the total time, as shown in Figure 2.

As the time window $\Delta t_j$ increases, the tangential angle curves become less jumpy and more continuous, resulting in an increased overlap ratio $OV_{i,j}$. However, excessively large $\Delta t_j$ can lead to delayed early warning information. When the overlap ratio reaches 80%, the curves are considered sufficiently similar. Therefore, when $OV_{i,j} \ge 80\%$, the corresponding $\Delta t_j$ is selected as the optimal time window, and the corresponding tangential angle $\alpha_{i,j}$ is taken as the output value.

4. Warning level

The PEW method utilizes a longer SATW compared to the time window in traditional methods. Additionally, the average velocity during the entire monitoring process exceeds that of the second stage (constant deformation). As a result, the tangential angle warning values for each hazardous stage in the PEW method will be slightly smaller than those presented in Table 1. Furthermore, the tangential angle values during the constant deformation stage should not be fixed at 45°, but rather represented as a range of values. The warning criteria for landslide early warning using the PEW method are illustrated in Figure 3.

### 2.2.2 | AEW method

Landslides typically evolve from initial deformation to final collapse, during which the affected area expands, as illustrated in

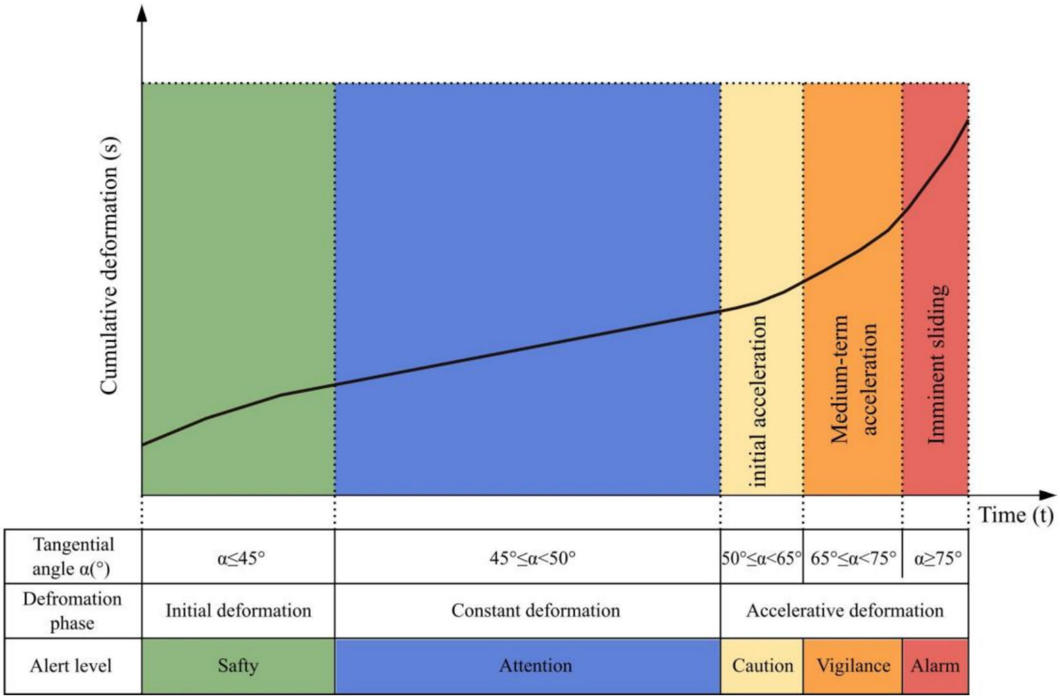


**FIGURE 3** Tangential angle and associated PEW levels.

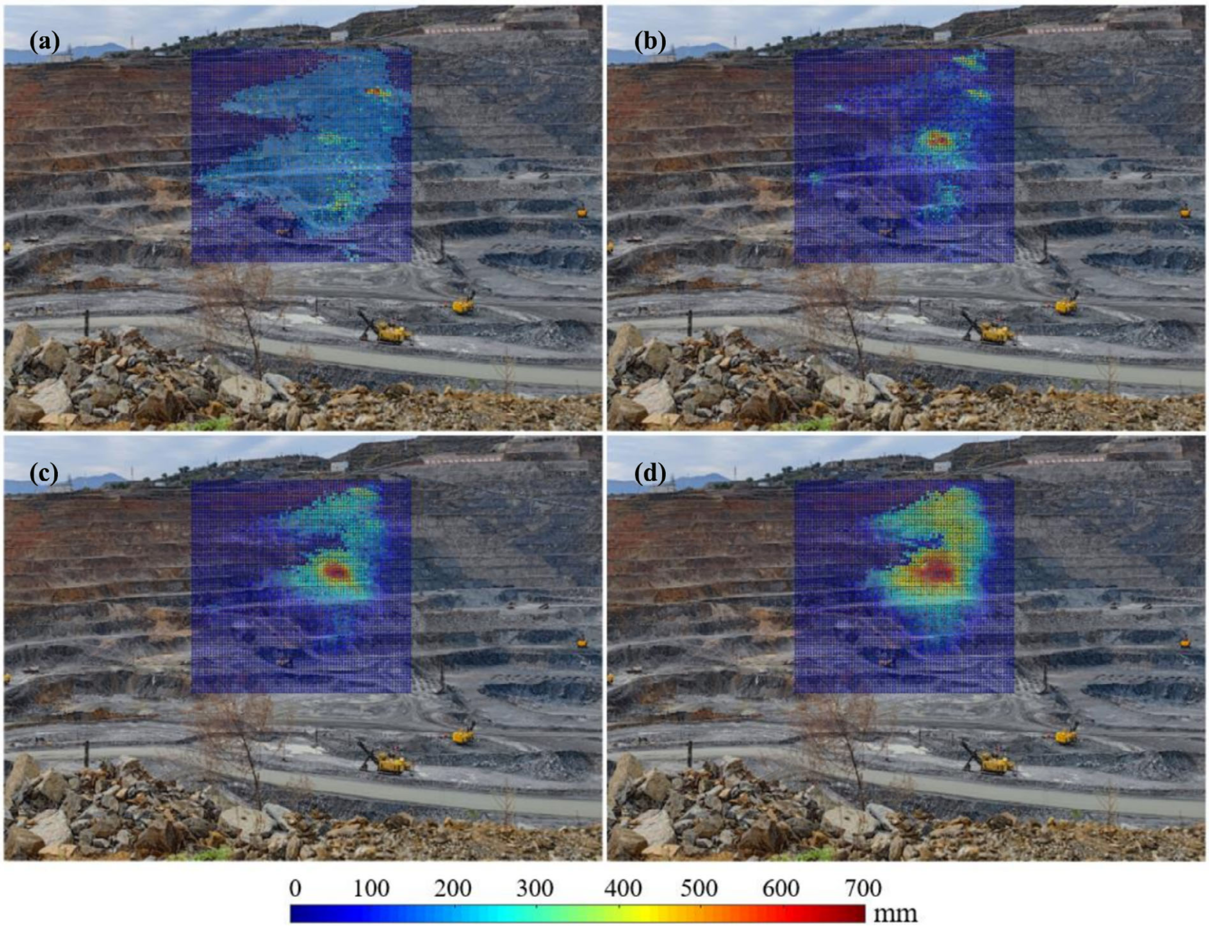


**FIGURE 4** Schematic diagram of deformation evolution during landslide progression from (a) to (d).

Figure 4. The AEW method involves two main steps: first, defining deformation thresholds; second, calculating the area of pixels exceeding these thresholds at each time step, which forms the area–time curve. The tangential angle of this curve is determined using the SATW method, and warnings are issued based on the angle.

The method requires a reasonable initial deformation threshold. In our observations, if the threshold is too low, the area–time curve rapidly reaches its maximum value and then levels off. Conversely, if the threshold is set too high, it becomes challenging to identify early deformation. Figure 5 shows area–time curves for different deformation thresholds. Only the information from the phase of curve variation is significant. Thus, it is clear that relying on a single threshold, whether large or small, has limitations in effectively capturing the entire monitoring process.

Given that a single threshold is insufficient for practical applications, we propose a dynamic multiple-threshold approach. Based on the maximum accumulated deformation $S_{max}$ in the monitoring area, $N$ deformation thresholds, denoted as $\{S_k\}_{k=1}^{N}$, are designed. Typically, the cumulative deformation before landslide failure can span several orders of magnitude, from millimetres to metres. If a fixed deformation increment is used throughout the monitoring process, $N$ can become excessively large, wasting computational resources. To optimize, when the cumulative deformation is below 100 mm, thresholds are selected with a 10 mm increment; above 100 mm, increments of 100 mm are used. The selection principle for the thresholds is simplified in Figure 6. This multiple-threshold approach ensures efficient use of computational resources while capturing the entire deformation process.

For each threshold $S_k$, the average area expansion rate $B_{k,i}$ at time $t_i$ is calculated as follows:

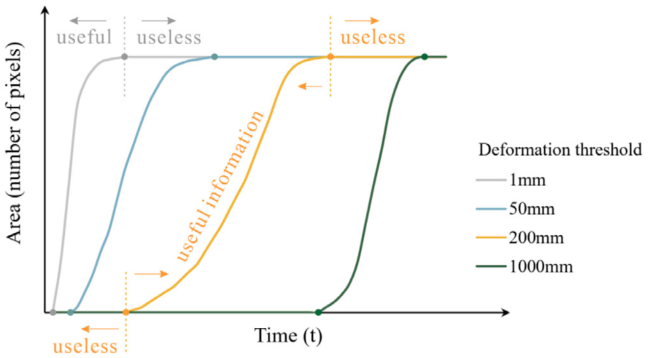


**FIGURE 5** Area–time curves for different deformation thresholds.

$$B_{k,i} = \frac{A_{k,i} - A_{k,1}}{t_i - t_1} \tag{9}$$

where $A_{k,i}$ refers to the area of accumulated deformation exceeding $S_k$ at time $t_i$.

Next, the cumulative deformation $S_i$ is divided by the average rate $B_{k,i}$ to obtain $T_{k,i}$, which has the same units as time:

$$T_{k,i} = \frac{A_{k,i}}{B_{k,i}} \tag{10}$$

The tangential angle $\alpha_{k,i}$ on the $A_{k,i}$-$t$ curve is given by

$$\alpha_{k,i} = arctan\frac{\Delta T}{\Delta t} = arctan\frac{T_{k,i} - T_{k,i-n}}{t_i - t_{i-n}} = arctan\frac{A_{k,i} - A_{k,i-n}}{B_{k,i}\cdot(t_i - t_{i-n})} \tag{11}$$

where $\Delta t$ is the time window calculated using the SATW method.

At time $t_i$, the deformation threshold $S_k$ corresponds to a tangential angle $\alpha_{k,i}$. By applying this to all $N$ deformation thresholds, we obtain $N$ tangential angles, and the maximum value $\alpha_i$ is selected as the output (Equation 12).

$$\alpha_i = \max\{\alpha_{k,i}\}_{k=1}^{N} \tag{12}$$

Finally, the warning is issued based on the relationship between the tangential angle and the warning level, as specified in Table 2.

## 3 | APPLICATION

The Jianshan landslide, located in the mining area of Loubo County, Shanxi Province, China, began to deform in September 2021 due to mining activities and eventually failed completely on October 6. The geological setting of the area is relatively simple, primarily consisting of exposed Paleoproterozoic Yuanjiacun banded iron formations. To ensure the safety of personnel involved in construction and mining operations, the GB-InSAR system was employed for continuous

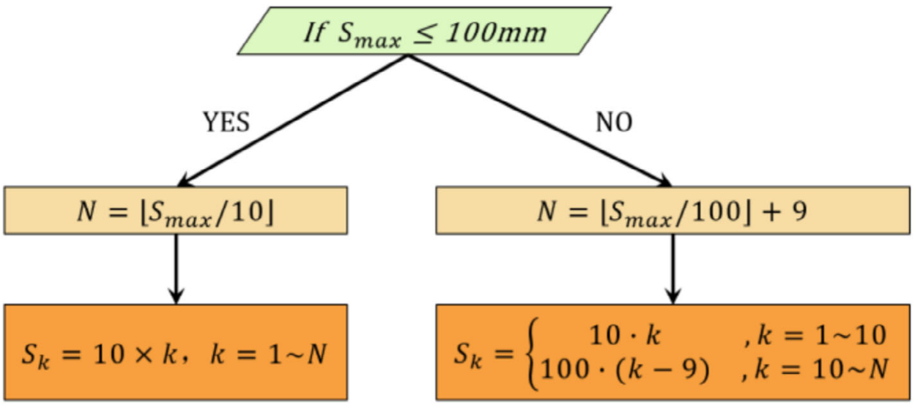


**FIGURE 6** Principle of deformation threshold selection $S_k$.

**TABLE 2** Tangential angle and associated AEW levels.

| Tangential angle | $\alpha < 40^\circ$ | $40^\circ \le \alpha < 50^\circ$ | $50^\circ \le \alpha < 75^\circ$ | $75^\circ \le \alpha < 80^\circ$ | $\alpha > 80^\circ$ |
|---|---|---|---|---|---|
| Warning level | Safety | Attention | Caution | Vigilance | Alarm |

monitoring of the Jianshan landslide over a 7-day period, from 17:19 on 3 October 2021 to 04:56 on 10 October 2021 (Figure 7).

Figure 8 provides a panoramic view of the mining area and the Jianshan landslide from the radar's perspective, captured on 30 October 2021. It clearly highlights areas of significant deformation and damage.

The GB-InSAR system employed is a ground-based multiple-input multiple-output (GB-MIMO) radar developed by Reco Sensing Technology Co., Ltd., affiliated with Suzhou Institute of Technology. The GB-MIMO radar is a specialized form of ground-based synthetic aperture radar (GB-SAR), utilizing waveform diversity to synthesize a large aperture through a multi-antenna structure. Detailed specifications of the radar system are provided in Table 3.

Radar images obtained from the GB-MIMO system were processed using the persistent scatterer (PS) interferometry technique to generate deformation maps of the Jianshan landslide. PS interferometry utilizes radar signal phase information reflected from stable scatterers on the Earth's surface to detect and measure subtle surface displacements with high precision (Li et al., 2024, 2025). Figure 9 illustrates the surface deformation of the Jianshan landslide, as derived from the GB-InSAR data. The total monitoring area consists of 3016 pixels, with maximum deformation exceeding 3 m. Figure 9a shows the cumulative deformation map at the final monitoring time. During the monitoring period, deformation data were recorded every 8 min, totalling 1150 time steps. Figure 9b presents the deformation–time curve for the point with the maximum deformation. Despite the relatively short monitoring period, the landslide failure process was successfully captured. Notably, the monitoring data for the point with the maximum deformation were used as a reference point to validate the performance of the PEW method, while the AEW method utilized data from all 3016 pixels.

**FIGURE 7** GB-InSAR system employed in the emergency monitoring.

## 4 | RESULTS

### 4.1 | The PEW method

A comparison between the PEW method and the traditional tangential angle method allows for an assessment of the PEW method's performance. However, a challenge arises: The traditional method is typically applicable to scenarios where a distinct constant velocity phase can be identified. In contrast, GB-InSAR monitored open-pit mines often exhibit very rapid deformation, and the monitoring periods are usually short, making it difficult to quickly ascertain the constant velocity phase. Therefore, the traditional method used in this section has been adapted. Specifically, the monitoring frequency is employed as the time interval, and the average velocity calculated during the constant velocity phase is replaced by the overall average velocity across the entire monitoring period. The displacement–time series of a representative point on the Jianshan landslide (Figure 9b) served as the case study data to test the performance of both the PEW method and the traditional method. The displacement–time curve featured a monitoring interval of 8 min. The key distinction lies in the fact that the traditional method utilizes the monitoring interval directly as the time window in its calculation formula, whereas the PEW method employs the SATW method to convert this into the required time window.

First, the traditional method was employed for the calculation, yielding the tangential angle–time curve depicted in Figure 10. As evidenced by the figure, the tangential angle exhibits significant

**TABLE 3** Radar system parameters.

| Parameters | Value |
|---|---|
| Band | Ku |
| Wavelength | 1.85 cm |
| Carrier frequency | 16.2 GHz |
| Bandwidth | 400 MHz |
| Sampling rate | 25 MHz |
| Resolution | 0.3 m(R) × 9.0 mrad(A) |
| Power | 40 W |
| Detection range | 30–4000 m |

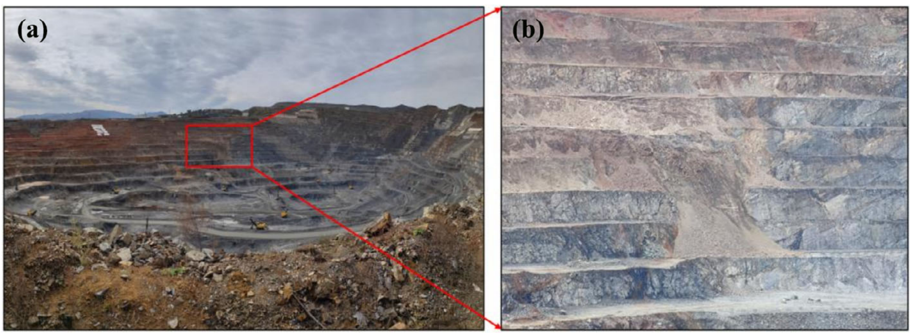


**FIGURE 8** Field photos. (a) Panoramic view of the mine pit. (b) Jianshan landslide.

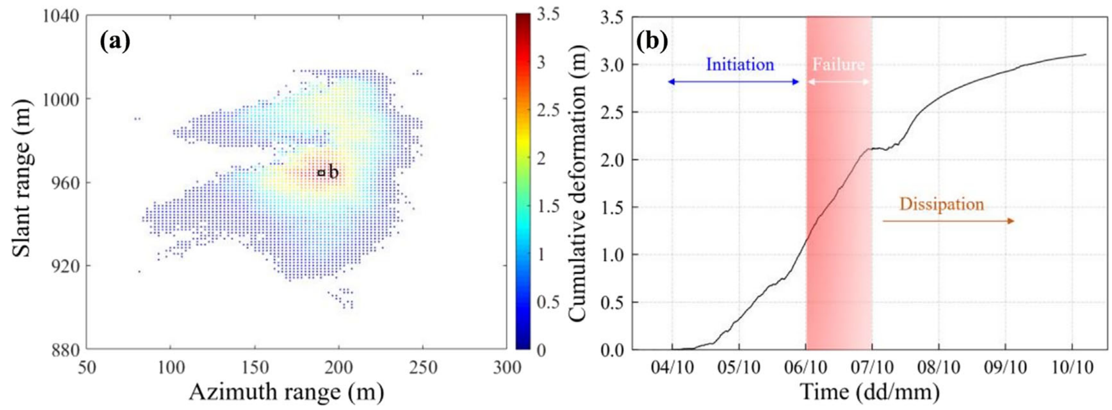


**FIGURE 9** Deformation of the Jianshan landslide. (a) Cumulative deformation of the surface scene. (b) Deformation–time curve of the typical point.

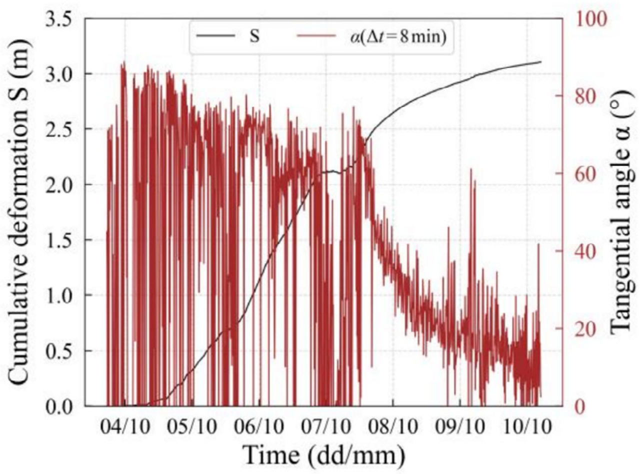


**FIGURE 10** Tangential angle–time curve based on the traditional method.

fluctuations, with its value reaching zero on 163 occasions. Since the early warning system relies directly on these tangential angle values, such abrupt changes could potentially trigger false alarms or missed alarms during the warning process.

Subsequently, the PEW method was utilized to calculate the tangential angle–time curve. To determine the optimal window, we tested a range of time intervals from 1 to 10 h, substituting them into Equation (5) for SATW calculation. The corresponding tangential angle–time curves for these windows are shown in Figure 11. A comparison of these 10 curves clearly reveals that the frequency and amplitude of abrupt changes in the tangent angle curves are closely related to the size of the time window. Figure 12 illustrates the number of zero-crossings in the tangential angle curve under different time windows. As the time window increases, the number of zero-crossings decreases monotonically, suggesting an inverse relationship between the number of abrupt changes and the window size.

From Figure 11e, it is evident that excessively large time windows introduce a delay in the warning system. Furthermore, extreme values in the tangential angle curve shift towards the middle value, which may compromise the accuracy of early warning predictions.

The overlap rates of tangential angle curves under various time windows are also calculated and presented in Figure 13. The overlap rate for 1-h and 2-h windows is below 65%, but it increases significantly as the time window expands, exceeding 90% for larger windows. Based on the principle of optimizing the time window, the goal is to minimize abrupt changes while avoiding a delay in the warning system. Therefore, a time window with an overlap rate greater than 80% is selected, and a 4-h time window is deemed optimal for this dataset.

The optimal time window (4 h) was applied to Equation (5) for the calculation of the tangential angle, and the early warning thresholds were established as shown in Figure 3. The early warning levels, as determined by the PEW method, are presented in Figure 14. During the initial stage of deformation, the PEW method issued vigilance and alarm-level warnings. These warnings persisted until October 6, just before the overall collapse of the landslide. After October 7, the warning level gradually decreased to attention and safety. This progression closely corresponds with the field observations, further validating the effectiveness of the proposed early warning system.

To compare the performance advantages of the PEW method with the traditional method, early warning results based on varying time windows were generated (Figure 15). As illustrated, early warning levels derived from the traditional method, using an 8-min monitoring interval as the time window, exhibited frequent fluctuations in the short term, with warning levels changing up to several times within a single day. Given that landslide deformation is a geotechnical process involving energy release, it is unreasonable for the tangential angle to fluctuate drastically and frequently within such a short timeframe. Therefore, frequent daily changes in the warning level are implausible.

Upon examining the warning results for different time windows in Figure 15, it is evident that as the time window increases, the abrupt fluctuations in the warning results decrease, and the temporal evolution becomes more coherent and logically consistent. However, as the time window continues to increase, a lag in the warning information becomes apparent. For instance, on October 6, the vigilance warning appears earlier with a smaller time window. Therefore, both excessively large and small time windows are unsuitable.

Figure 16 displays the percentage of time spent at each warning level across different time windows. For the 8-min time window, the distribution of warning levels is as follows: Safety (55%), Attention (6%), Caution (14%), Vigilance (15%) and Alarm (10%). As the time

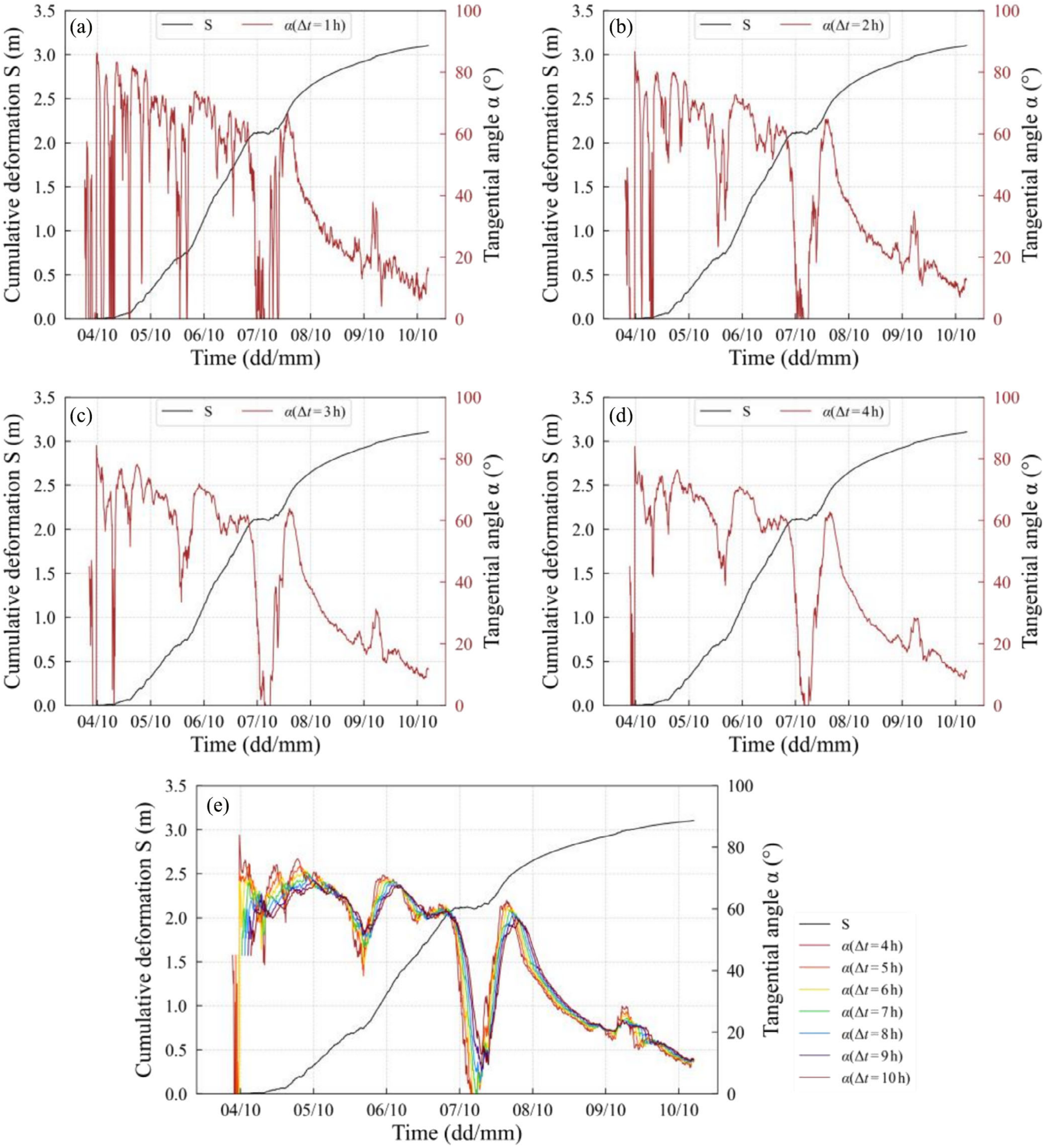


**FIGURE 11** Tangential angle–time curve under multiple time windows. (a) 1 h. (b) 2 h. (c) 3 h. (d) 4 h. (e) 4–10 h.

window expands, the proportion of Safety decreases and eventually stabilizes, while the percentage of Alarm decreases until it reaches zero. The total duration of Vigilance and Alarm initially stabilizes (from 8 min to 4 h) and then gradually declines. This pattern corresponds to the behavior of the tangential angle fluctuations: A smaller time window captures more extreme values, resulting in a higher frequency of Safety and Alarm warnings. In contrast, larger time windows average the extreme tangential angle values, leading to a reduction in the duration of Vigilance and Alarm warnings. The total duration of Vigilance and Alarm decreases when the time window exceeds 4 h, demonstrating that a 4-h window effectively reduces warning fluctuations while mitigating information lag. This validates the effectiveness of the SATW method, confirming that the PEW method significantly improves upon the traditional tangential angle warning approach.

## 4.2 | The AEW method

In the cumulative deformation graph of the Jianshan landslide surface (Figure 9a), the maximum cumulative deformation, $S_{max}$, was found to be 3103.9 mm. Following the selection principle outlined in Figure 6, 40 deformation thresholds were established. For each threshold $S_k$, the area exceeding this deformation was calculated, resulting in 40 area–time curves (Figure 17).

As illustrated in Figure 17, the curve with the lowest deformation threshold begins to increase first. Over time, additional curves emerge, indicating an increase in both the magnitude of landslide deformation and the area of the deformation zone. Between October 6 and 7, several curves with higher deformation thresholds exhibited a sharp rise, closely aligning with our on-site observations of comprehensive landslide failure. After October 8, the curves corresponding to smaller deformation thresholds remained largely stable, while those with higher thresholds continued to experience gradual increases. This suggests that the overall extent of landslide deformation ceased to expand, although localized areas of intense deformation within the landslide mass continued to experience movement.

The 4-h time window was calculated using the SATW method and subsequently applied to Equations (9)–(12) to obtain the corresponding tangential angle–time curves for each area–time curve (Figure 18). For each time point in Figure 18, 40 tangential angle values were generated, from which the maximum value was selected as the output tangential angle according to Equation (12). Subsequently, the warning level was determined based on the thresholds provided in Table 2, resulting in the warning levels depicted in Figure 19.

From Figure 18, it can be observed that during the initial monitoring phase, the maximum tangential angle values occur on curves with smaller deformation thresholds. As time progresses and the landslide develops, the location of the maximum tangential angle shifts to curves with higher deformation thresholds. Notably, after October 7th, the tangential angle values corresponding to the yellow curves with smaller deformation thresholds experience a sharp decline, remaining within the safety warning range. In contrast, curves with larger deformation thresholds continue to exhibit substantial tangential angle values. This figure clearly demonstrates that the maximum tangential angle at each moment throughout the process shifts among different deformation threshold curves. In the early stages, curves with smaller deformation thresholds serve as effective early warning indicators,

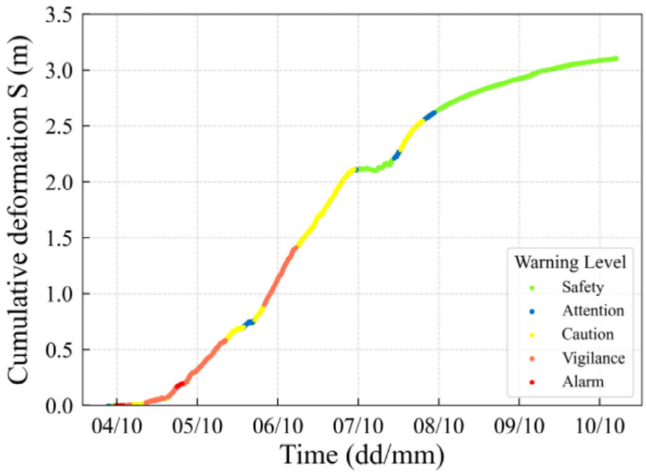


**FIGURE 14** Warning level based on PEW method.

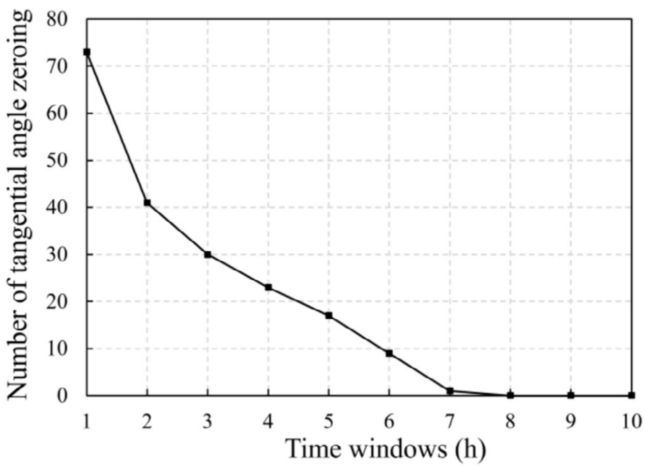


**FIGURE 12** Number of tangential angle zero-crossings under multiple time windows.

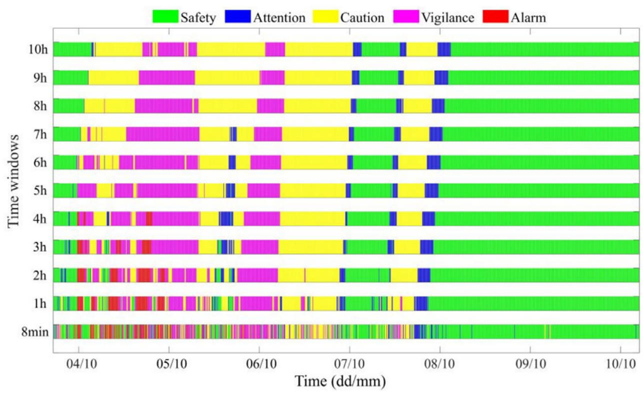


**FIGURE 15** Early warning level under different time windows.

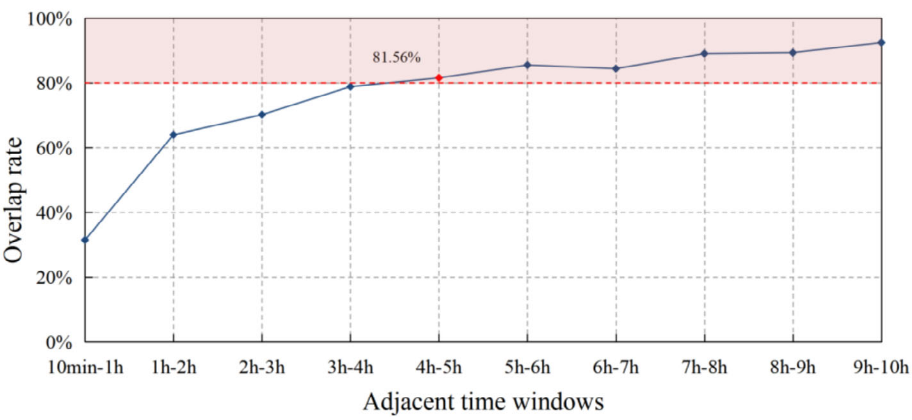


**FIGURE 13** Overlap rates of tangential angle curves under multiple time windows.

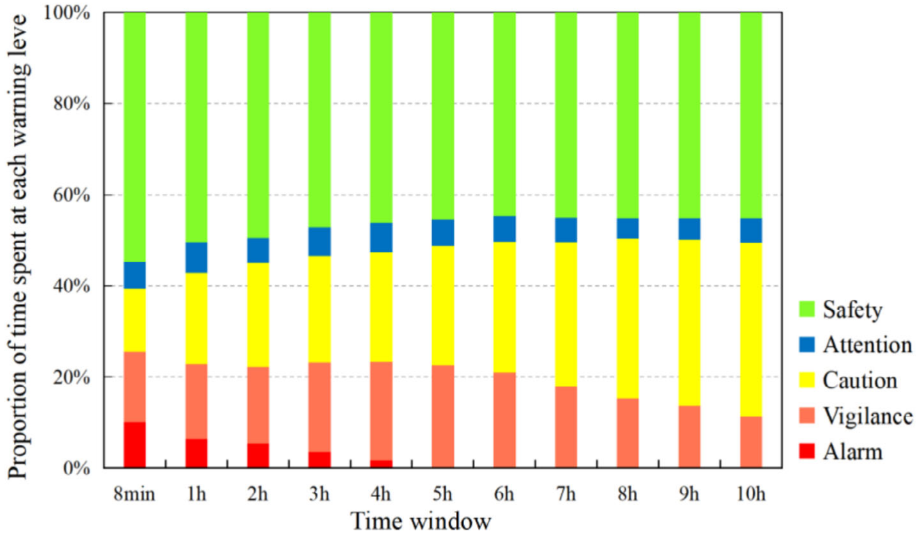


**FIGURE 16** Proportion of time spent at each warning level for different time windows.

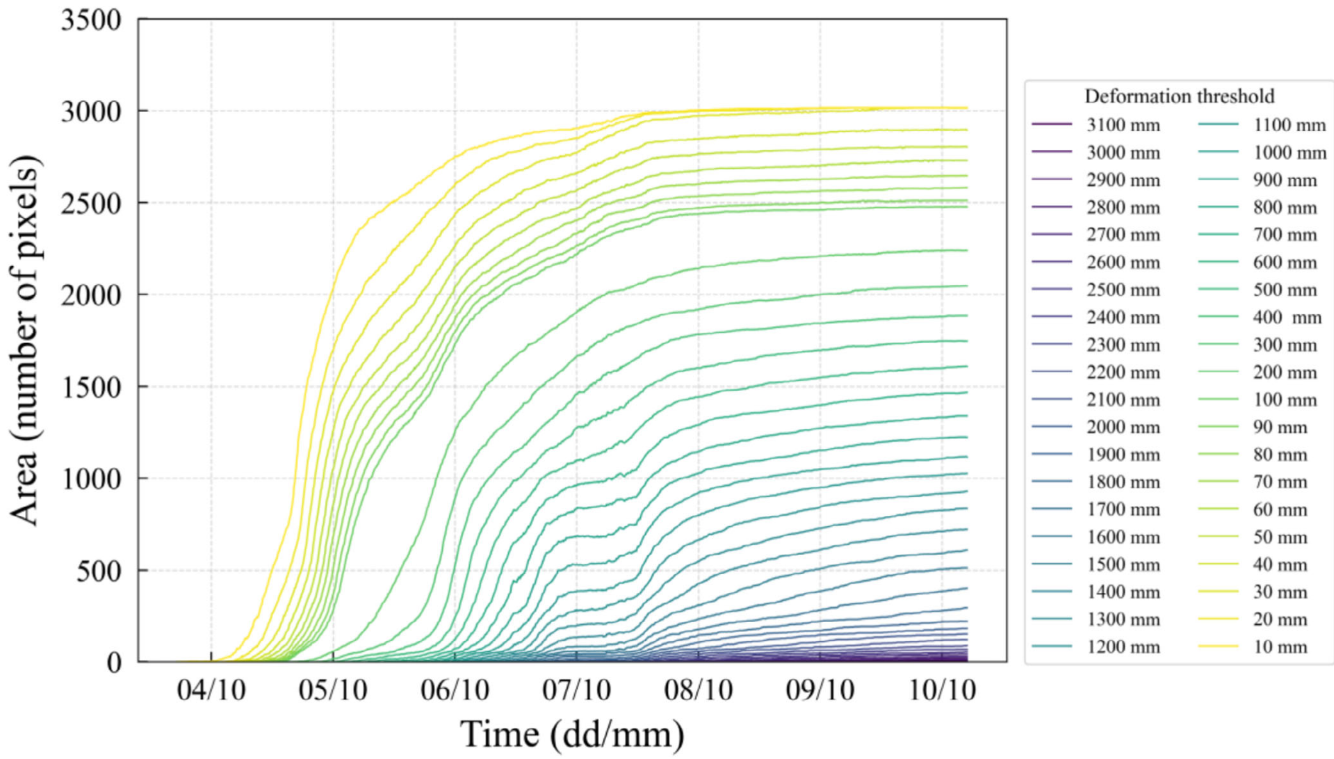


**FIGURE 17** Area–time curves for all deformation thresholds.

while in the later stages, curves with larger deformation thresholds assume this role. The dynamic multiple-threshold approach designed in this study holds significant importance.

### 4.3 | The final output integrated early warning level

The PEW method focuses on the evolution of the maximum deformation point, while the AEW method emphasizes changes in the deformation zone. Both methods' warning levels reflect the hazard status of the slope, but due to their differing analytical perspectives, the warning levels at each time point may vary (Figure 20a). As shown in the figure, during the deformation and failure development phase of the slope (before October 6), the warning levels derived from both the PEW and AEW methods are similar. However, after the overall landslide occurred on October 6, the warning levels of the two methods diverge significantly in the following days. This is mainly because, after the overall failure of the landslide, the deformation rate sharply decreases, and the PEW method immediately lowers the warning level to a safe state. Meanwhile, the landslide continues to exhibit some deformation in certain areas, which is captured by the AEW method.

Our proposed integrated warning model takes into account the danger status of the landslide body from a point to a surface perspective. Therefore, at each time point, the more severe warning between those issued by the PEW and AEW methods was selected as the final warning result (Figure 20b).

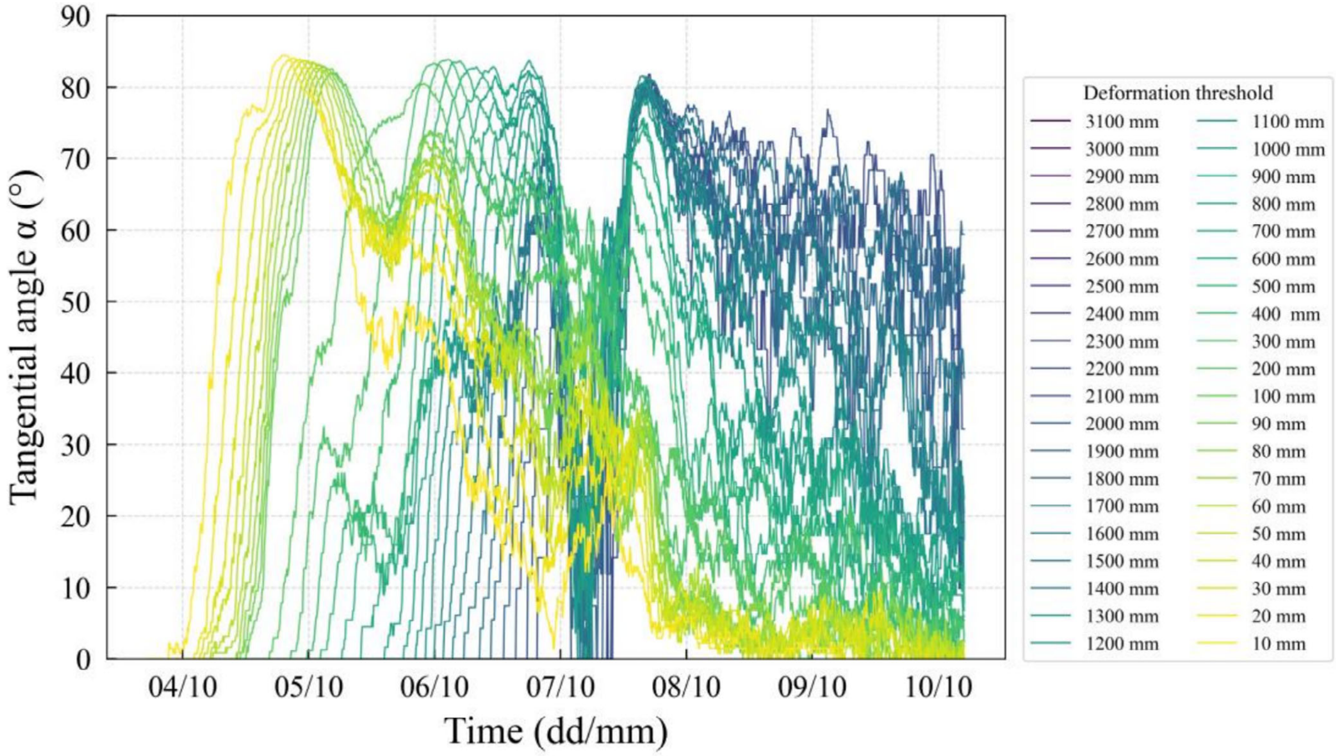


**FIGURE 18** Tangential angle–time curves.

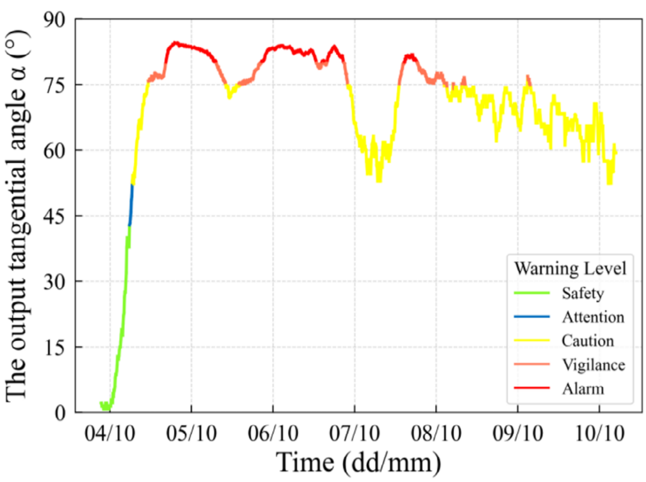


**FIGURE 19** Warning level based on AEW method.

## 5 | DISCUSSION

### 5.1 | Applicability, advantages and integration strategy of the early warning method

Based on the high spatio-temporal resolution deformation data obtained by GB-InSAR, this study successfully developed and validated a landslide early warning framework that integrates both PEW and AEW methods. It is particularly noteworthy that, considering the high suddenness of mine slope failures and the extremely short available response time (Rezaei & Mousavi, 2024), this study specifically optimized the lower threshold for the tangential angle in the PEW method (Figure 3). Although this setting is lower than the common thresholds found in traditional tangential angle methods (Chen et al., 2024), this optimization significantly reduced the frequency of false and missed alarms, as demonstrated by the comparison in Figures 10 and 11d. This improvement is of great significance for addressing the insufficient warning effectiveness of traditional methods in high-risk scenarios like mining (Kemajl et al., 2024).

Regarding applicability, the proposed framework demonstrates good generalization capability and technical compatibility. The PEW method, requiring only a single-point deformation series, can be readily integrated into existing point-based monitoring networks like GNSS (Huang et al., 2023) and crack meters (Thohari et al., 2024), offering a new pathway to enhance the warning capability of existing infrastructure. The core contribution of the AEW method lies in its fundamental solution to the inherent limitations of point-based monitoring—namely, the inability to capture the spatial heterogeneity of hazards and the potential omission of critical unstable areas between sensor networks (Hosseini et al., 2023). By evaluating the size of the deformation zone and the spatio-temporal evolution stage of the failure, the AEW method enables effective diagnosis of the overall slope stability. This aligns with the current trend in landslide monitoring shifting from 'point' to 'area' (Casagli et al., 2023).

Regarding the integration of PEW and AEW, this study adopts the 'highest-level principle' as a preliminary strategy, aiming to simplify the decision-making process. However, we are fully aware that such a linear integration model may lead to overestimation or underestimation of warning levels in specific scenarios. This, in fact, reveals a common challenge in the fusion of multi-source monitoring information (Feng et al., 2021). For instance, when AEW consistently indicates 'Alert' while PEW transitions from 'Alert' to 'Safe', this may suggest localized deformation stabilization while the overall risk continues to accumulate. In such cases, maintaining the 'Alert' level, while a prudent measure, highlights the need for future research to develop

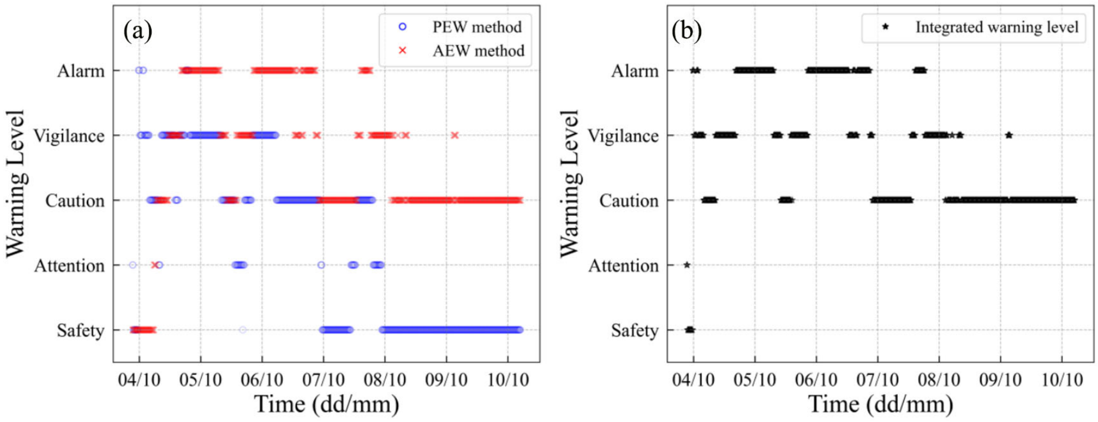


**FIGURE 20** Early warning levels. (a) Comparison of PEW method and AEW method. (b) Integrated warning level.

non-linear dynamic weight integration models (Wang et al., 2025). These models would assign different confidence levels to PEW and AEW based on distinct stages of landslide evolution. Ultimately, a robust early warning system must be an organic combination of theoretical models, on-site verification and expert experience (Rokhideh et al., 2025).

### 5.2 | Basis, sensitivity and generalizability exploration of threshold setting

Threshold setting is crucial for translating the tangential angle early warning method from theory into practice. As confirmed by studies such as Ge et al. (2023) and Liu, Zhang, et al. (2024), thresholds are not immutable. Such variations profoundly reflect fundamental differences in the geotechnical properties, failure mechanisms and evolutionary processes of different types of landslides (Fan et al., 2019). Therefore, this study advocates that thresholds should be customized according to the type of hazard—an approach gradually gaining consensus in the research community (Tomás et al., 2024).

A prominent advantage of the proposed framework lies in its ability to dynamically capture the complete spatio-temporal evolution chain of landslides, from 'local deformation' to 'regional propagation' and finally to 'global failure'. This makes it particularly suitable for slope types characterized by progressive surface expansion, such as loess slopes and mine slopes, whose evolutionary patterns align closely with the 'progressive failure' model described in (Chen et al., 2021). In contrast, its warning efficacy may be relatively limited for landslides dominated by steady-state creep along fixed slip surfaces, as these rely more on accurate characterization of slip surface behavior than on the detection of surficial expansion (Pfeiffer et al., 2023).

It must be acknowledged that the thresholds in this study were primarily fine-tuned based on commonly cited ranges in the literature and empirical adjustments for specific cases, inevitably introducing a degree of subjectivity. This underscores that threshold determination itself constitutes a vast and complex research topic. Future work should focus on statistical analysis of large sample cases to establish threshold databases for different geomechanical models, thereby advancing early warning parameters from an 'empirical' basis towards 'standardized' and 'theoretically grounded' practices.

### 5.3 | Understanding the limitations of GB-InSAR technology and future perspectives

The GB-InSAR technique retrieves surface displacement by measuring the deformation projection along the radar line of sight (LOS), a principle that inherently leads to geometric distortion in the monitoring data (He et al., 2024). In areas where the direction of deformation significantly deviates from the LOS, the underestimation of the actual displacement becomes particularly pronounced. This may result in an underestimation of the calculated tangential angle during the slope acceleration phase, potentially leading to delayed warnings—a common challenge faced by all single-LOS InSAR technologies in early warning applications (Bayik et al., 2024).

Nevertheless, the integrated framework proposed in this study exhibits a certain inherent robustness to such errors. This is because the AEW approach focuses more on the spatial propagation pattern of unstable areas, which relies less on absolute deformation values compared to the PEW method. This implies that even if the LOS displacement value of an individual point is biased, as long as the relative spatial variations and propagation trends remain reliable, AEW can still effectively identify the overall instability risk.

To fundamentally overcome this technical limitation, we recommend deploying multiple GB-InSAR instruments in future emergency monitoring scenarios to form a multi-angle observation network. This aligns with the current frontier approach of deriving true three-dimensional deformation fields through multi-platform and multi-geometry InSAR techniques (Samadzadegan et al., 2025). Utilizing multi-baseline interferometry for real-time 3D deformation monitoring (Liu, Zeng, et al., 2024) will provide more accurate input data for warning models, which is undoubtedly an essential direction for developing next-generation high-precision landslide early warning systems.

## 6 | CONCLUSIONS

The PEW method employs the SATW algorithm to calculate the tangent angle values of the deformation time series, thereby enabling effective early warning. Compared to traditional tangent angle methods, the PEW method significantly reduces abrupt fluctuations in early warning results and enhances outcome reliability. Furthermore, the AEW method represents the first innovative early warning approach based on area deformation monitoring. It effectively identifies expansion trends of landslide deformation areas, providing a novel perspective for monitoring and early warning methodologies. The early warning results derived from the AEW method complement those of the PEW method, and their combination offers a more comprehensive warning signal. While the proposed method establishes a framework integrating landslide acceleration and expansion, certain details within this framework require further research and refinement. Additional case studies remain necessary to validate and optimize the method, ensuring its robustness and applicability across various geological scenarios.

## AUTHOR CONTRIBUTIONS

**Ting Xiao:** Conceptualization; funding acquisition; methodology; writing—initial draft; writing—reviewing and editing. **Weiming Tian:** Conceptualization; investigation; resources; writing—reviewing and editing. **Samuele Segoni:** Methodology; writing—reviewing and editing. **Emanuele Intrieri:** Methodology; writing—reviewing and editing. **Yunkai Deng:** Investigation; software; writing—initial draft; writing—reviewing and editing. **Yunping Liao:** Investigation.

## ACKNOWLEDGEMENTS

The work described in this paper was funded by grants from the National Natural Science Foundation of China (Project No. 42307275), the Natural Science Foundation of Hunan Province, China (Project No. 2024JJ6498) and the Technology Innovation Center of Geohazards Automatic Monitoring (Project No. TICG-K2024008).

## DATA AVAILABILITY STATEMENT

The data that support the findings of this study are available from the corresponding author upon reasonable request.

## ORCID

*Emanuele Intrieri* https://orcid.org/0000-0002-9227-4409
*Yunkai Deng* https://orcid.org/0000-0003-2765-2976

## REFERENCES

Bai, D., Lu, G., Zhu, Z., Zhu, X., Tao, C. & Fang, J. (2022) A hybrid early warning method for the landslide acceleration process based on automated monitoring data. *Applied Sciences*, 12(13), 6478. Available from: https://doi.org/10.3390/app12136478

Bardi, F., Raspini, F., Ciampalini, A., Kristensen, L., Rouyet, L., Lauknes, T., et al. (2016) Space-borne and ground-based InSAR data integration: the Åknes test site. *Remote Sensing*, 8(3), 237. Available from: https://doi.org/10.3390/rs8030237

Bayik, C., Abdika, S. & Gül, M. (2024) Mass movement evaluation in deformed clastic rock with InSAR technique. *Earth Surface Processes and Landforms*, 49(2), 875–886. Available from: https://doi.org/10.1002/esp.5716

Carlà, T., Tofani, V., Lombardi, L., Raspini, F., Bianchini, S., Bertolo, D., et al. (2019) Combination of GNSS, satellite InSAR, and GBInSAR remote sensing monitoring to improve the understanding of a large landslide in high alpine environment. *Geomorphology*, 335, 62–75. Available from: https://doi.org/10.1016/j.geomorph.2019.03.014

Casagli, N., Intrieri, E., Tofani, V., Gigli, G. & Raspini, F. (2023) Landslide detection, monitoring and prediction with remote-sensing techniques. *Nature Reviews Earth & Environment*, 4(1), 51–64. Available from: https://doi.org/10.1038/s43017-022-00373-x

Chen, Q., Huang, W. & Li, J. (2024) Landslide early warning based on improved tangential angle and displacement rate: a case study of the Leijiashan landslide in Shimen county, Hunan province. *Chinese Journal of Geological Hazard & Control*, 35(5), 133–140. Available from: https://doi.org/10.16031/j.cnki.issn.1003-8035.202303041

Chen, S., Xiong, L., Duan, J. & Tang, G. (2021) Formation of asymmetrical loess gullies in the northeastern Loess Plateau of China. *Earth Surface Processes and Landforms*, 46(4), 758–774. Available from: https://doi.org/10.1002/esp.5062

Cignetti, M., Godone, D., Notti, D., Giordan, D., Bertolo, D., Calò, F., et al. (2023) State of activity classification of deep-seated gravitational slope deformation at regional scale based on Sentinel-1 data. *Landslides*, 20(12), 2529–2544. Available from: https://doi.org/10.1007/s10346-023-02114-7

Crosta, G. & Agliardi, F. (2002) How to obtain alert velocity thresholds for large rockslides. *Physics and Chemistry of the Earth, Parts A/B/C*, 27(36), 1557–1565. Available from: https://doi.org/10.1016/S1474-7065(02)00177-8

Crosta, G.B., Agliardi, F., Rivolta, C., Alberti, S. & Dei Cas, L. (2017) Long-term evolution and early warning strategies for complex rockslides by real-time monitoring. *Landslides*, 14(5), 1615–1632. Available from: https://doi.org/10.1007/s10346-017-0817-8

Cruden, D. & Varnes, J. (1996) Landslide types and processes. In: *Landslides: investigation and mitigation, transportation research board (National Research Council)*. Washington, DC: National Academy Press.

Dick, G.J., Eberhardt, E., Cabrejo-Liévano, A.G., Stead, D. & Rose, N.D. (2015) Development of an early-warning time-of-failure analysis methodology for open-pit mine slopes utilizing ground-based slope stability radar monitoring data. *Canadian Geotechnical Journal*, 52(4), 515–529. Available from: https://doi.org/10.1139/cgj-2014-0028

Dixon, N., Smith, A., Flint, J.A., Khanna, R., Clark, B. & Andjelkovic, M. (2018) An acoustic emission landslide early warning system for communities in low-income and middle-income countries. *Landslides*, 15(8), 1631–1644. Available from: https://doi.org/10.1007/s10346-018-0977-1

Dumperth, C., Rohn, J., Fleer, A. & Xiang, W. (2016) Local-scale assessment of the displacement pattern of a densely populated landslide, utilizing finite element software and terrestrial radar interferometry: a case study on Huangtupo landslide (P.R. China). *Environmental Earth Sciences*, 75(10), 880. Available from: https://doi.org/10.1007/s12665-016-5475-y

Eberhardt, E., Clague, J. & Stead, D. (2012) Landslide monitoring: the role of investigative monitoring to improve understanding and early warning of failure. In: *Landslides: types, mechanisms and modeling*. Cambridge, UK: Cambridge University Press.

Fan, X., Rossiter, D.G., van Westen, C.J., Xu, Q. & Görüm, T. (2014) Empirical prediction of coseismic landslide dam formation. *Earth Surface Processes and Landforms*, 39(14), 1913–1926. Available from: https://doi.org/10.1002/esp.3585

Fan, X., Xu, Q., Liu, J., Subramanian, S.S., He, C., Zhu, X., et al. (2019) Successful early warning and emergency response of a disastrous rockslide in Guizhou province, China. *Landslides*, 16(12), 2445–2457. Available from: https://doi.org/10.1007/s10346-019-01269-6

Feng, Y., Hu, J., Duan, R. & Chen, Z. (2021) Credibility assessment method of sensor data based on multi-source heterogeneous information fusion. *Sensors (Basel)*, 21(7), 2542. Available from: https://doi.org/10.3390/s21072542

Ge, Q., Sun, H., Liu, Z. & Wang, X.J.G.J. (2023) A data-driven intelligent model for landslide displacement prediction. *Geological Journal*, 58(6), 2211–2230. Available from: https://doi.org/10.1002/gj.4675

Gu, X., Nie, W., Geng, J., Yuan, C., Zhu, T. & Zheng, S.J.S.E.R. (2023) Road slope monitoring and early warning system integrating numerical simulation and image recognition: a case study of Nanping, Fujian, China. *Stochastic Environmental Research and Risk Assessment*, 37(10), 3819–3835. Available from: https://doi.org/10.1007/s00477-023-02482-5

Han, H., Shi, B., Zhang, C.-C., Sang, H., Huang, X. & Wei, G.J.A.G. (2023) Application of ultra-weak FBG technology in real-time monitoring of landslide shear displacement. *Acta Geotechnica*, 18(5), 2585–2601. Available from: https://doi.org/10.1007/s11440-022-01742-y

He, K., Lombardo, L., Chang, L., Sadhasivam, N., Hu, X., Fang, Z., et al. (2024) Investigating earthquake legacy effect on hillslope deformation using InSAR-derived time series. *Earth Surface Processes and Landforms*, 49(3), 980–990. Available from: https://doi.org/10.1002/esp.5746

Hosseini, K., Reindl, L., Raffl, L., Wiedemann, W. & Holst, C. (2023) 3D landslide monitoring in high spatial resolution by feature tracking and histogram analyses using laser scanners. *Remote Sensing*, 16(1), 138. Available from: https://doi.org/10.3390/rs16010138

Huang, G., Du, S. & Wang, D. (2023) GNSS techniques for real-time monitoring of landslides: a review. *Satellite Navigation*, 4(1), 5. Available from: https://doi.org/10.1186/s43020-023-00095-5

Intrieri, E., Bardi, F., Fanti, R., Gigli, G., Fidolini, F., Casagli, N., et al. (2017) Big data managing in a landslide early warning system: experience from a ground-based interferometric radar application. *Natural Hazards and Earth System Sciences*, 17(10), 1713–1723. Available from: https://doi.org/10.5194/nhess-17-1713-2017

Intrieri, E., Raspini, F., Fumagalli, A., Lu, P., Del Conte, S., Farina, P., et al. (2017) The Maoxian landslide as seen from space: detecting precursors of failure with Sentinel-1 data. *Landslides*, 15(1), 123–133. Available from: https://doi.org/10.1007/s10346-017-0915-7

Jibson, R.W., Harp, E.L. & Michael, J.A. (2000) A method for producing digital probabilistic seismic landslide hazard maps. *Engineering Geology*, 58(3-4), 271–289. Available from: https://doi.org/10.1016/S0013-7952(00)00039-9

Ju, N., Huang, J., He, C., Van Asch, T.W.J., Huang, R., Fan, X., et al. (2020) Landslide early warning, case studies from southwest China. *Engineering Geology*, 279, 105917. Available from: https://doi.org/10.1016/j.enggeo.2020.105917

Kemajl, Z., Stojance, M., Gzim, I. & Ledi, M.L. (2024) Comprehensive analysis of the mining accident forecasting and risk assessment methodologies: case study–Stanterg mine. *Mining Of Mineral Deposits*, 18(2), 11–17. Available from: https://doi.org/10.33271/mining18.02.011

Li, B., Peng, B., Chang, L., Niu, R. & Li, Y. (2024) Unveiling spatial pattern in slope units-based landslides using a data-driven GAMM and InSAR techniques. *Remote Sensing Letters*, 15(10), 1085–1095. Available from: https://doi.org/10.1080/2150704X.2024.2406031

Li, Y., Jiang, W., Li, B., Tian, T., Li, Y., Wang, N., et al. (2025) Revealing the slip distribution and seismogenic structure of the magnitude 6.2 Jishishan (Gansu) earthquake in 2023 through multi-source InSAR observations. *Geo-spatial Information Science*, 1–12. Available from: https://doi.org/10.1080/10095020.2024.2440613

Liu, D., Zeng, B., Xu, H., Ai, D. & Yuan, J. (2024) Three-dimensional deformation monitoring of landslides based on combination of two-track InSAR observations and pixel-level surface-parallel flow model. *International Journal of Remote Sensing*, 45(22), 8380–8404. Available from: https://doi.org/10.1080/01431161.2024.2399334

Liu, F., Yang, Z., Deng, W., Yang, T., Zhou, J., Yu, Q., et al. (2024) Rock landslide early warning system combining slope stability analysis, two-stage monitoring, and case-based reasoning: a case study. *Bulletin of Engineering Geology and the Environment*, 80, 8433–8451. Available from: https://doi.org/10.1007/s10064-021-02461-6

Liu, S., Zhang, P., Tang, Q., Wu, S. & Huang, Y. (2024) A novel safety early warning methodology for pipelines under landslide geological hazard. *Journal of Pipeline Systems Engineering and Practice*, 15(1), 04023050. Available from: https://doi.org/10.1061/JPSEA2.PSENG-1529

Macciotta, R., Hendry, M. & Martin, C.D. (2015) Developing an early warning system for a very slow landslide based on displacement monitoring. *Natural Hazards*, 81(2), 887–907. Available from: https://doi.org/10.1007/s11069-015-2110-2

Meng, Q., Li, W., Raspini, F., Xu, Q., Peng, Y., Ju, Y., et al. (2020) Time-series analysis of the evolution of large-scale loess landslides using InSAR and UAV photogrammetry techniques: a case study in Hongheyan, Gansu province, northwest China. *Landslides*, 18(1), 251–265. Available from: https://doi.org/10.1007/s10346-020-01490-8

Nava, L., Tordesillas, A., Qian, G. & Catani, F.J.L. (2024) Displacement residuals reveal landslide regime shifts. *Landslides*, 22(1), 1–16. Available from: https://doi.org/10.1007/s10346-024-02353-2

Pecoraro, G., Calvello, M. & Piciullo, L. (2018) Monitoring strategies for local landslide early warning systems. *Landslides*, 16(2), 213–231. Available from: https://doi.org/10.1007/s10346-018-1068-z

Pfeiffer, J., Zieher, T. & Schneider-Munta, B. (2023) Slope stability evolution of a deep-seated landslide considering a constantly deforming topography. *Earth Surface Processes and Landforms*, 48(5), 923–939. Available from: https://doi.org/10.1002/esp.5527

Rezaei, M. & Mousavi, S.Z.S. (2024) Slope stability analysis of an open pit mine with considering the weathering agent: field, laboratory and numerical studies. *Engineering Geology*, 333, 107503. Available from: https://doi.org/10.1016/j.enggeo.2024.107503

Rokhideh, M., Fearnley, C. & Budimir, M. (2025) Multi-hazard early warning systems in the Sendai framework for disaster risk reduction: achievements, gaps, and future directions. *International Journal of Disaster Risk Science*, 16(1), 103–116. Available from: https://doi.org/10.1007/s13753-025-00622-9

Saito, M. (1969) Forecasting time of slope failure by tertiary creep. In: Proceedings of the 7th International Conference on Soil Mechanics and Foundation Engineering, Mexico City, Mexico. Citeseer, 677–683.

Saito, M. & Uesawa, H.J.L. (1966) Prediction of slope failure period. *Landslides*, 2(2), 7–12. Available from: https://doi.org/10.3313/jls1964.2.2_7

Samadzadegan, F., Toosi, A. & Dadrass, J.F. (2025) A critical review on multi-sensor and multi-platform remote sensing data fusion approaches: current status and prospects. *International Journal of Remote Sensing*, 46(3), 1327–1402. Available from: https://doi.org/10.1080/01431161.2024.2429784

Strząbała, K., Ćwiąkała, P. & Puniach, E.J.R.S. (2024) Identification of landslide precursors for early warning of hazards with remote sensing. *Remote Sensing*, 16(15), 2781. Available from: https://doi.org/10.3390/rs16152781

Tan, W., Wang, Y., Huang, P., Qi, Y., Xu, W., Li, C., et al. (2023) A method for predicting landslides based on micro-deformation monitoring radar data. *Remote Sensing*, 15(3), 826. Available from: https://doi.org/10.3390/rs15030826

Thohari, A.N.A., Karima, A., Santoso, K. & Rahmawati, R. (2024) Crack detection in building through deep learning feature extraction and machine learning approach. *Journal of Applied Informatics and Computing*, 8(1), 1–6. Available from: https://doi.org/10.30871/jaic.v8i1.7431

Tian, W., Zhao, Z., Hu, C., Wang, J. & Zeng, T. (2019) GB-InSAR-based DEM generation method and precision analysis. *Remote Sensing*, 11(9), 997. Available from: https://doi.org/10.3390/rs11090997

Tomás, R., Zeng, Q., Lopez-Sanchez, J.M., Zhao, C., Li, Z., Liu, X., et al. (2024) Advances on the investigation of landslides by space-borne synthetic aperture radar interferometry. *Geo-spatial Information Science*, 27(3), 602–623. Available from: https://doi.org/10.1080/10095020.2023.2266224

Wang, H., Zhong, P., Xiu, D., Zhong, Y., Peng, D. & Xu, Q. (2022) Monitoring tilting angle of the slope surface to predict loess fall landslide: an on-site evidence from Heifangtai loess fall landslide in Gansu province, China. *Landslides*, 19(3), 719–729. Available from: https://doi.org/10.1007/s10346-021-01727-0

Wang, L., Qiu, H., Zhou, W., Zhu, Y., Liu, Z., Ma, S., et al. (2022) The post-failure spatiotemporal deformation of certain translational landslides may follow the pre-failure pattern. *Remote Sensing*, 14(10), 2333. Available from: https://doi.org/10.3390/rs14102333

Wang, Z., Fang, X., Zhang, W., Wang, L., Wang, K. & Chen, C. (2025) Dynamic intelligent prediction approach for landslide displacement based on biological growth models and CNN-LSTM. *Journal of Mountain Science*, 22(1), 71–88. Available from: https://doi.org/10.1007/s11629-024-9113-y

Woods, A., Macciotta, R., Hendry, M.T., Stewart, T. & Marsh, J. (2021) Updated understanding of the deformation characteristics of the Checkerboard Creek rock slope through GB-InSAR monitoring. *Engineering Geology*, 281, 105974. Available from: https://doi.org/10.1016/j.enggeo.2020.105974

Wu, S., Hu, X., Zheng, W., Berti, M., Qiao, Z. & Shen, W. (2021) Threshold definition for monitoring Gapa landslide under large variations in reservoir level using GNSS. *Remote Sensing*, 13(24), 4977. Available from: https://doi.org/10.3390/rs13244977

Xiao, T., Huang, W., Deng, Y., Tian, W. & Sha, Y. (2021) Long-term and emergency monitoring of Zhongbao landslide using space-borne and ground-based InSAR. *Remote Sensing*, 13(8), 1578. Available from: https://doi.org/10.3390/rs13081578

Xu, Q., Peng, D., Zhang, S., Zhu, X., He, C., Qi, X., et al. (2020) Successful implementations of a real-time and intelligent early warning system for loess landslides on the Heifangtai terrace, China. *Engineering Geology*, 278, 105817. Available from: https://doi.org/10.1016/j.enggeo.2020.105817

Xu, Q., Yuan, Y., Zeng, Y. & Hack, R. (2011) Some new pre-warning criteria for creep slope failure. *SCIENCE CHINA Technological Sciences*, 54(S1), 210–220. Available from: https://doi.org/10.1007/s11431-011-4640-5

Yin, Y., Wang, H., Gao, Y. & Li, X. (2010) Real-time monitoring and early warning of landslides at relocated Wushan town, the Three Gorges Reservoir, China. *Landslides*, 7(3), 339–349. Available from: https://doi.org/10.1007/s10346-010-0220-1

Zhang, J., Tang, H., Li, C., Gong, W., Zhou, B. & Zhang, Y.J.L. (2024) Deformation stage division and early warning of landslides based on the statistical characteristics of landslide kinematic features. *Landslides*, 21(4), 717–735. Available from: https://doi.org/10.1007/s10346-023-02192-7

Zhang, J., Tang, H., Tan, Q., Mao, M., Zhou, B. & Zhang, Y.J.A.G. (2024) A generalized early warning criterion for the landslide risk assessment: deformation probability index (DPI). *Acta Geotechnica*, 19(5), 2607–2627. Available from: https://doi.org/10.1007/s11440-023-02199-3

**How to cite this article:** Xiao, T., Tian, W., Segoni, S., Intrieri, E., Deng, Y. & Liao, Y. (2026) Integrated early warning method for landslide acceleration and expansion based on GB-InSAR monitoring. *Earth Surface Processes and Landforms*, 51(1), e70226. Available from: https://doi.org/10.1002/esp.70226